

**Peptides**

# Enzyme Induced Solid-Like Condensates Formation of Engineered Peptide in Living Cells for Prostate Cancer Inhibition

Ying Li, Tengyan Xu, Yaoting Li, and Huaimin Wang\*

**Abstract:** This work describes the rational design and synthesis of hepsin-recognized amphiphilic-branched peptides (**DMN-SIPL**) that can form solid condensates through liquid–liquid phase separation (LLPS) upon enzymatic reaction. The peptide forms solid-like condensates both in vitro and in living cells, triggered by type-II membrane-associated serine peptidase, hepsin, whose overexpression determines prostate cancer progression. Specifically, integrating self-assembly, hepsin hydrolysis, and hepsin-binding domain generates a branched substrate that acts as a precursor for enzyme-induced LLPS. Upon binding hepsin on the cell membrane, **DMN-SIPL** forms condensates initiated by hepsin-induced self-assembly. The prostate cancer cells then uptake these condensates via lipid raft-mediated endocytosis. The entrapped hepsin in the condensates further hydrolyzes the **DMN-SIPL** to stabilize the intracellular condensates. Structure–activity relationship reveals the importance of enzyme-binding motif, enzyme-recognized motif, and the self-assembly motif. Mechanistic studies indicate that the resulting solid-like condensates modulate cancer cell metabolism by inhibiting hepsin upstream protein activation and downstream signal transduction, ultimately inducing cancer cell growth inhibition selectively. As a first example, this work investigates enzymatic LLPS condensate formation in living cells, paving the way to generate functional synthetic biomolecular condensates through LLPS for biomedical applications.

## Introduction

Liquid–liquid phase separation (LLPS) is a phenomenon that can drive the formation of condensates.<sup>[1–3]</sup> Differences in

intermolecular and intramolecular forces within condensates lead to significant variations in their properties.<sup>[4]</sup> The structure of condensates can range from highly fluid liquid states (droplets) to more viscous, viscoelastic, or solid-like state.<sup>[5–10]</sup> Recent advances in cell biology have revealed that various cellular compartments execute and modulate signal transduction through membraneless organelles, which concentrate relevant molecules to form biomolecule condensates through liquid–liquid phase separation.<sup>[11–15]</sup> Unlike membrane-bound structures, membraneless organelles allow for a more dynamic and flexible organization of cellular components, enabling rapid responses to cellular signals and environmental changes.

Aside from the views of the biologists that establish the correlation between condensates with biological functions,<sup>[9,16–19]</sup> chemists and material scientists are exploring the molecular principles governing the LLPS and engineering them for emerging applications.<sup>[9,20–28]</sup> For instance, Ulijn et al. introduced connected peptide modules that enable the controlled coexistence of self-assembled fibers within liquid condensates, enhancing the understanding of intracellular dynamics.<sup>[21]</sup> Yu's group demonstrated that hydrogen bond is crucial for the phase separation of mussel-derived adhesive peptides, informing the design of synthetic materials that mimic natural processes.<sup>[22]</sup> Abbas et al. focused on a short peptide synthon that facilitates liquid–liquid phase separation, laying the groundwork for developing biomimetic protocells.<sup>[20,23]</sup> Moreover, researchers have made significant strides in the development of condensates for cargo delivery, enhancing the efficiency of therapeutic agents.<sup>[29]</sup> For example, Miserez group explored phase-separating peptides for direct cytosolic delivery of therapeutics, demonstrating a novel mechanism for redox-activated release.<sup>[27]</sup> Hamachi et al. investigated how temporal stimulus patterns influenced the differentiation of synthetic dipeptide-based coacervates, contributing to the understanding of responsive biomimetic systems.<sup>[28]</sup> Additionally, Webber and his coworkers highlighted glucose-driven condensate formation in supramolecular peptide complexes, underscoring the potential for adaptive drug delivery systems.<sup>[9]</sup>

Although significant progress has been made in developing condensates formation and applying them in cargo delivery,<sup>[9,25–27,30]</sup> the reporting condensates formed by amphiphilic peptides are initially prepared in an abiotic system and then introduced into the biological system, which could lead to their dissociation before reaching the intended target after cellular uptake or dilution.<sup>[29]</sup> In contrast, cells inherently use in situ-formed condensates to control biological functions, such as cellular signal transduction, a

[\*] Y. Li, Dr. T. Xu, Y. Li, Dr. H. Wang

Key Laboratory of Precise Synthesis of Functional Molecules of Zhejiang Province, Department of Chemistry, School of Science, Institute of Natural Sciences, Westlake Institute for Advanced Study, Westlake University, No. 600 Dunyu Road, Hangzhou, Zhejiang 310024, China

E-mail: wanghuaimin@westlake.edu.cn

Dr. H. Wang

Westlake Laboratory of Life Sciences and Biomedicine, School of Life Sciences, Westlake University, Hangzhou, Zhejiang, China

 Additional supporting information can be found online in the Supporting Information section

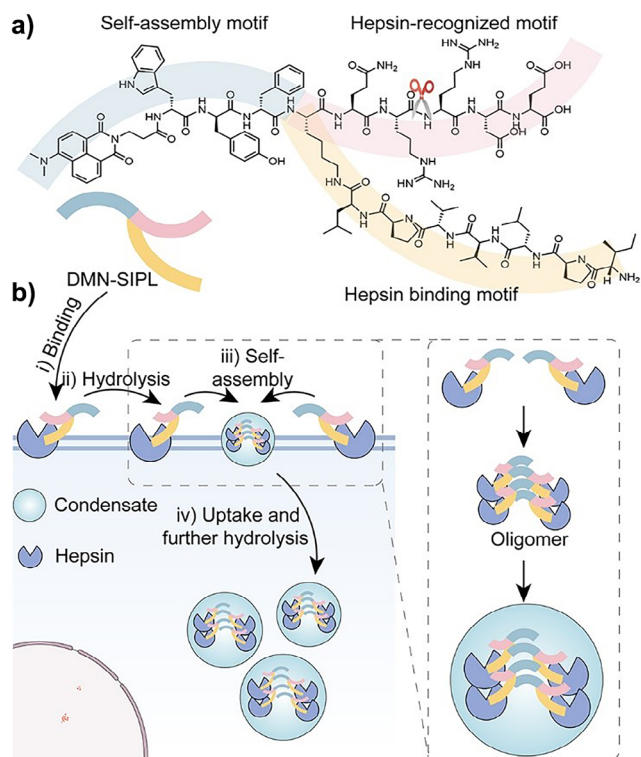


**Figure 1.** a) Molecular structure of **DMN-SIPL**. b) Schematic illustration of condensates formation in cells. i) **DMN-SIPL** binds to hepsin through the hepsin binding motif. ii) Enzyme-instructed hydrolysis occurs on cell membrane, producing hydrolysates with enhanced self-assembly property. iii) Peptide and hepsin first self-assemble into oligomers, which then recruit additional oligomers to form condensates through liquid–liquid phase separation at cell membrane. iv) The condensates are internalized by cells, where the peptides undergo further hydrolysis to stabilize the condensates in the cytoplasm.

capability that has not yet been fully realized in artificial systems.<sup>[31–36]</sup>

To address these limitations, we investigate the formation of enzyme-induced membraneless organelles in prostate cancer cells, demonstrating the potential of LLPS to modulate metabolic processes in a biologically relevant context. Hepsin is a multifunctional transmembrane serine protease that plays a key role in the occurrence and development of various tumors, particularly in prostate cancer and liver cancer.<sup>[37]</sup> The high expression of hepsin is significantly associated with poor prognosis, making it a potential target for cancer therapy.<sup>[38]</sup> Hepsin was selected as the regulatory factor for this system. As shown in Figure 1a, the formation of solid-like condensates of peptide on the cell membrane depends on the presence of specific peptide motifs: a self-assembly motif, a hepsin recognition motif, and a hepsin-binding motif. Upon binding to hepsin via the binding motif, the optimized peptide undergoes hydrolysis on the cell membrane, initiating condensates formation. These condensates are subsequently internalized by cells through cholesterol-dependent lipid raft. Within the cytoplasm, continued hydrolysis promotes condensates stability. Mechanistic studies indicate that the formed hepsin-peptide condensates inhibit the activation of upstream signaling proteins, thereby suppressing the hepsin-

signaling pathway. This suppression offers a potential strategy for condensates-based cancer therapy, as disrupting hepsin signaling can inhibit cell metastasis. The *in vitro* condensates formation experiment indicates that the balance of peptide–peptide interactions, peptide–enzyme interactions, and the hydrolysis ratio within the system is critical in enzyme-induced LLPS process. By exploring enzymatic LLPS condensates formation in living cells, this work establishes a foundation for developing functional synthetic biomolecular condensates in living cells through LLPS for biomedical applications.

## Results and Discussion

### Molecular Design and Selective Condensates Formation

To enhance peptide stability and promote LLPS in cells, we use *D*-type tryptophan–tyrosine–phenylalanine (*w-y-f*, lower case letters indicate a *D*-amino acid) as a self-assembly motif, which provides strong hydrophobic interactions and enzyme-resistance. The enzyme recognition motif, lysine–glutamine–arginine–arginine (KQRR), is derived from glutamine–arginine–arginine (QRR) sequence, facilitating recognition by hepsin.<sup>[39]</sup> Additionally, the hepsin binding sequence, leucine–proline–valine–valine–leucine–proline–isoleucine (LPVVLPI), ensures a high binding affinity to hepsin.<sup>[40]</sup> The inclusion of aspartic acid–glutamic acid (**D-E**) at the C-terminus imparts hydrophilicity to the peptide. Strong interaction between the peptide and hepsin, combined with  $\pi$ – $\pi$  interactions and hydrogen bonding, facilitate the occurrence of LLPS. We synthesized all the peptides by standard solid-phase (Fmoc) peptide chemistry (Scheme S1). After purifying all the precursors by high-performance liquid chromatography (HPLC), we used analytical HPLC and LC-MS to confirm their purity and identity.

To investigate condensates formation, LNCaP cells, a prostate cancer cell line characterized by high expression level of hepsin, alongside PC-3 cells, which exhibit low hepsin levels as a control.<sup>[41,42]</sup> Both two cell lines were co-incubated with **DMN-SIPL** (Figure S1) to assess selective LLPS formation. Confocal laser scanning microscopy (CLSM) results (Figure 2a) showed that the formation of rounded condensates in LNCaP cells after 12 h incubation, indicating that **DMN-SIPL** effectively induced phase separation in LNCaP cells. In contrast, in PC-3 cells, the peptide appeared as smaller dots in the cytoplasm, likely localized within lysosomes. We also assessed HepG2 cells, another hepsin high expression cells, and SK-OV-3 cells, one cell line with low expression level of hepsin. Different structures formed in HepG2 cells and SK-OV-3 cells (Figures S2 and S3). In HepG2 cells, the rounded structures formed by **DMN-SIPL** were significantly larger than those in SK-OV-3 cells. To investigate the subcellular location of **DMN-SIPL**, we conducted immunofluorescence staining for LAMP1, a lysosomal-associated membrane protein (Figures S4 and S5). The result showed that **DMN-SIPL** formed condensates in HepG2 cells, while in SK-OV-3 cells, it localized to lysosome. Additionally, imaging following LAMP1-RFP

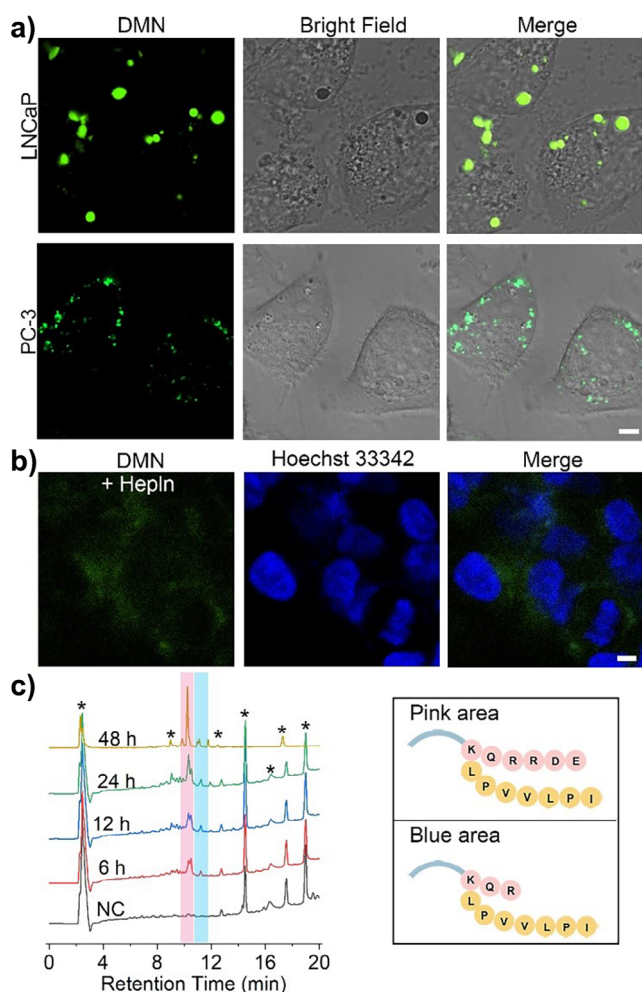


**Figure 2.** a) CLSM images of LNCaP cells and PC-3 cells treated with **DMN-SIPL** (100  $\mu\text{M}$ ) for 24 h. Scale bar is 5  $\mu\text{m}$ . b) CLSM images of LNCaP cells treated with **DMN-SIPL** (100  $\mu\text{M}$ ) in the presence of hepsin inhibitor (Hepln, 10  $\mu\text{M}$ ) for 12 h. Scale bar is 5  $\mu\text{m}$ . c) Analytic HPLC spectra of **DMN-SIPL** (100  $\mu\text{M}$ ) enzymatic products in cells after 6, 12, 24, and 48 h, respectively. Pink area indicates the original peptide, while blue area represents the hydrolysis product. Asterisks (\*) labels the peak of both cell systematic peaks and analytic HPLC systematic peaks. NC group represents cells without any treatment.

transfection (Figure S6) confirmed these findings, indicating the independence of **DMN-SIPL** in HepG2 cells.

To further evaluate the impact of hepsin activity on condensates formation, we co-incubated LNCaP cells with hepsin inhibitor Hepln. CLSM results (Figure 2b) showed complete inhibition of condensates formation, with only weak green fluorescence from **DMN-SIPL**, suggesting the importance of hepsin activity in this process. The enzymatic responsiveness of **DMN-SIPL** in cells was further investigated using an external standard method by analytic HPLC. These results (Figures 2c and S7) confirmed the presence of hydrolysate in cells. Specifically, **DMN-wyfK(LPVVLPI)QR** (blue area) was detected in cell lysates after 6 h of incubation. Peak of **DMN-SIPL** increased with increasing incubation time, indicating the time-dependent endocytosis of peptides. We calculated the concentration of **DMN-SIPL** and **DMN-KQR-**

**IPL** to determine the hydrolysis ratio of peptide in cells (Table S2). The hydrolysis ratio in cells is determined by the speed of **DMN-SIPL** endocytosis and hydrolysis, resulting in a consistent hydrolysis ratio of about 40% within 24 h, as observed in Figure S8. The release of the hydrophilic amino acid arginine resulted in hydrolysate with improved self-assembly capabilities, which contributes to LLPS occurrence in cells. Peptide stability is crucial for its applications in biological system.<sup>[43,44]</sup> Analytical HPLC results (Figure S9A,B) demonstrated that the degradation of the peptide **DMN-wyfK(LPVVL)QRRDE** became evident after 12 h of incubation in a culture medium containing 10% FBS. When the incubation time was extended to 48 h, the degradation ratio of the peptide reached 30%, indicating that 70% of the peptide remained in the culture medium (Figure S9C). These findings suggest that the branched peptide exhibits good stability. Based on the inhibitor co-incubation experiments and intracellular hydrolysis results, we conclude that hepsin activity and peptide hydrolysis ratio are critical determinants of the LLPS process within cells, highlighting the importance of the chemical design in this context.

To validate the condensates component in cells, we first conducted immunofluorescence (IF) analysis of hepsin. The IF result (Figure 3a) indicated that **DMN-SIPL** co-localized with the membrane protein hepsin to form condensates on cell membrane, with an overlap coefficient ( $r$ ) of 0.68 (Figures 3b, S10, and S11). With increased incubation time, the co-localization of hepsin and **DMN-SIPL** improved, yielding the  $r$  value of 0.76, suggesting a cooperative interaction that facilitates LLPS in cells. IF result also demonstrated that hepsin as an important component participated into the condensates formation. To further investigate the LLPS process, LNCaP cells were treated with **DMN-SIPL** for living cell imaging. Notably, condensates were observed on cell membrane after just 2 h (video clip S1). Although most of the peptide remained localized around the cell membrane with weak fluorescence intensity, indicating an initial binding process between **DMN-SIPL** and hepsin. Pull-down experiment was performed with biotin labeled peptide to demonstrate that peptide could bind to hepsin in cells (Figures S12 and S13). After 6 h of incubation, condensates appeared both around the cell membrane and within the cytoplasm, demonstrating that **DMN-SIPL** interacted with hepsin at the membrane before undergoing phase separation and entering the cytoplasm (Figure 3c).

To determine whether **DMN-SIPL** was sequestered in lysosomes or formed condensates in cytoplasm, we employed LysoTracker to stain acidic organelles. CLSM images (Figures 3d and S14) revealed that **DMN-SIPL** condensates did not co-localize with lysosomes, regardless of whether the incubation period was 12 or 24 h, indicating that these condensates existed independently in the cytoplasm as membraneless organelles. Various endocytosis inhibitors were tested to elucidate the potential mechanisms of peptide uptake, including low temperature (4  $^{\circ}\text{C}$ ), methyl- $\beta$ -cyclodextrin ( $\text{M}\beta\text{-CD}$ ) for cholesterol depletion,<sup>[45,46]</sup> sodium azide ( $\text{NaN}_3$ ) as an energy-dependent endocytosis inhibitor,<sup>[45,47]</sup> amiloride for pinocytosis inhibition<sup>[45,48]</sup> and chlorpromazine for clathrin-mediated endocytosis inhibition.<sup>[45,49]</sup> CLSM and quantification results

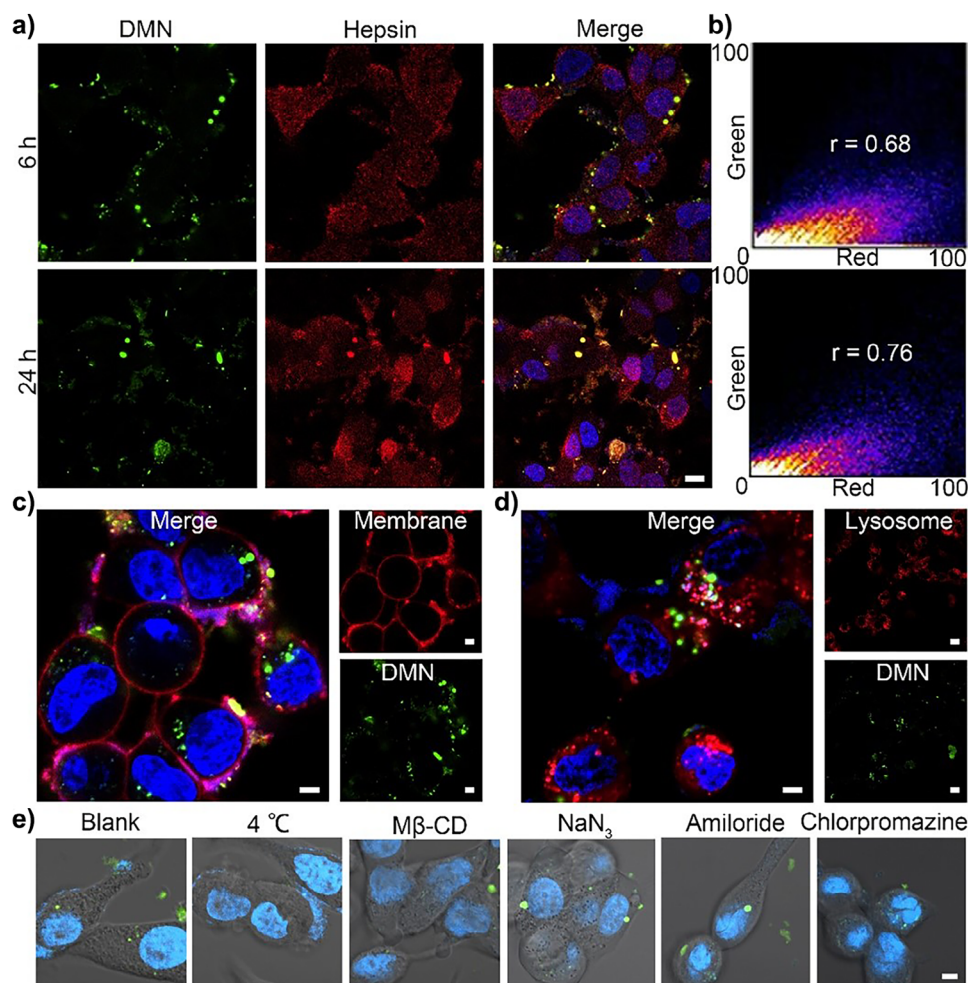


**Figure 3.** a) Immunofluorescence images of LNCaP cells treated with **DMN-SIPL** (100  $\mu\text{M}$ ) for 6 and 24 h. Red fluorescence represents hepsin and green fluorescence indicates **DMN-SIPL**. Scale bar is 10  $\mu\text{m}$ . b) Scatterplots showing the co-localization extent between **DMN-SIPL** and hepsin from the merged image from (a). Membraneless organelle formation and endocytosis of **DMN-SIPL** in cells. c) CLSM images of LNCaP cells treated with **DMN-SIPL** (100  $\mu\text{M}$ ) for 6 h. Cell membrane stained in red and nuclei stained with Hoechst 33342. Scale bar is 5  $\mu\text{m}$ . d) CLSM images of LNCaP cells treated with **DMN-SIPL** (100  $\mu\text{M}$ ) for 12 h. Lysosome was stained with LysoTracker Deep Red. Scale bar is 5  $\mu\text{m}$ . e) CLSM images of LNCaP cells pre-incubated with various endocytic inhibitors, then incubated with **DMN-SIPL** (100  $\mu\text{M}$ ) for 2 h. Scale bar is 5  $\mu\text{m}$ . Blank group represents cells without inhibitor pre-incubation but only **DMN-SIPL** treatment.

(Figures 3e and S15) indicated that only low temperature and  $\text{M}\beta\text{-CD}$  inhibited cellular uptake of **DMN-SIPL**. Low temperature inhibits all energy-dependent endocytosis and affects membrane fluidity. In contrast,  $\text{NaN}_3$  did not impact peptide uptake, suggesting that the uptake of **DMN-SIPL** does not rely on energy-dependent endocytosis.  $\text{M}\beta\text{-CD}$  depleted cholesterol from the cell membrane, blocking **DMN-SIPL** uptake and indicating that it entered cells through cholesterol-dependent lipid raft,<sup>[27,47]</sup> rather than traditional endocytic pathway, thus avoiding endosomal escape.<sup>[49]</sup>

#### Driving Force of LLPS and Property of Condensates

To verify condensates formation, we constructed condensates in vitro by co-incubating **DMN-SIPL** with hepsin. This resulted in liquid-liquid phase separation, leading to the formation of condensed condensates with size ranging from

1 to 5  $\mu\text{m}$  (Figure 4a). The appearance of a visible opaque substance at the bottom of the tube confirmed condensates formation through LLPS. The turbidity results with different hepsin incubation times showed increased turbidity with hepsin incubation, demonstrating the LLPS of **DMN-SIPL** (Figure S16). Notably, neither individual **DMN-SIPL** peptide nor hepsin alone were capable of forming condensates (Figures 4a and S17), highlighting the necessity of their interaction for LLPS.

To evaluate the contributions of the three peptide motifs to condensates formation, we synthesized several control peptides: the self-assembly mutant **DMN-GGGK(LPVVLP)** **QRRDE (DMN-GIPL)**, which lacked critical hydrophobic residues necessary for self-assembly; the hepsin-binding site mutant **DMN-wyfkQRRDE (DMN-S)**, which altered the sequence required for hepsin binding; and the hepsin recognition site mutant **DMN-wyfk(LPVVLP)** **GGRDE (DMN-SGIPL)** (Figures S18–S20). Notably, the

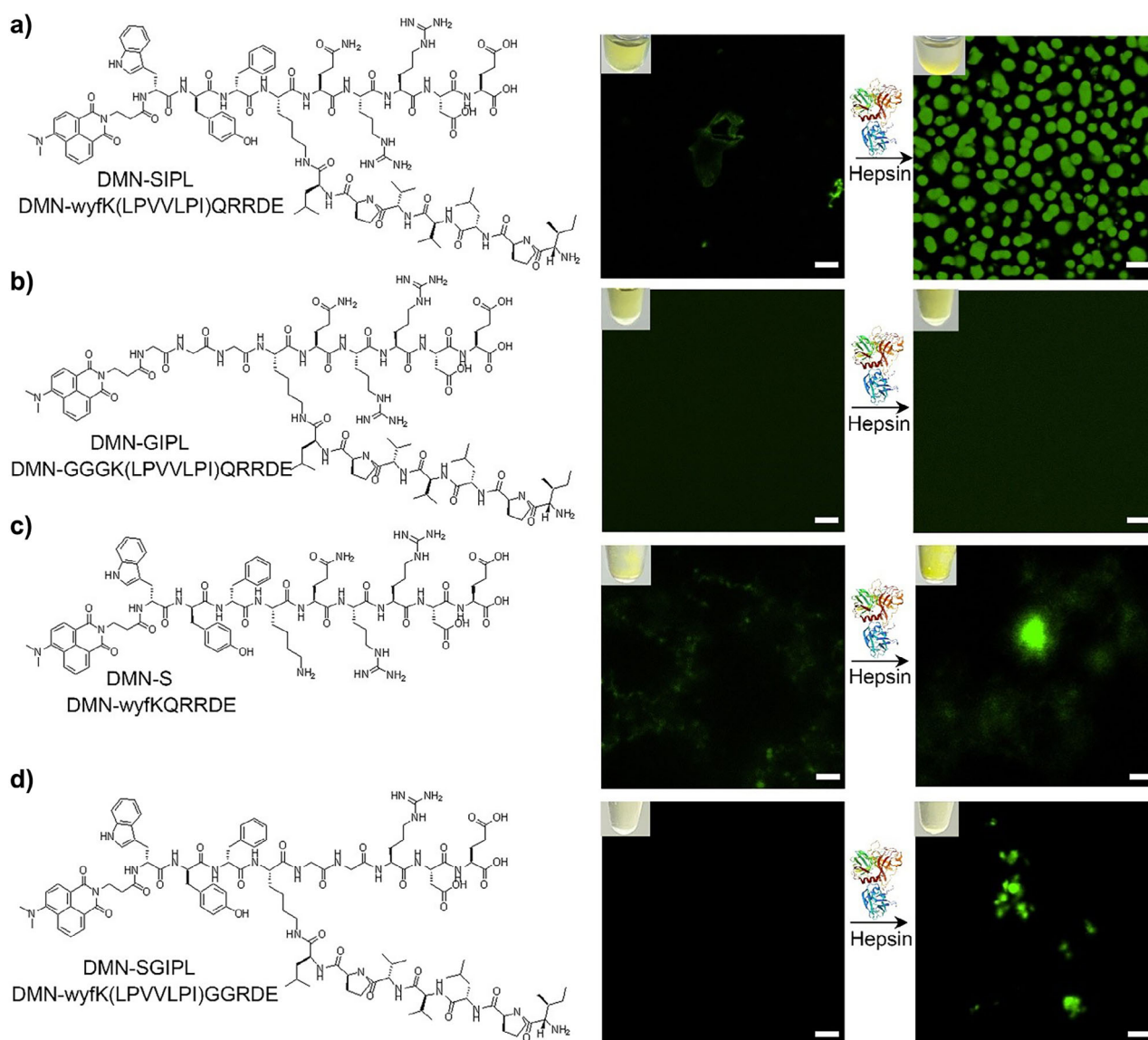


**Figure 4.** Molecular structure and confocal images of a) DMN-wyfK(LPVVLP)QRRDE (**DMN-SIPL**), b) DMN-GGGK(LPVVLP)QRRDE (**DMN-GIPL**), c) DMN-wyfKQRRDE (**DMN-S**), and d) DMN-wyfK(LPVVLP)GGRDE (**DMN-SGIPL**) treated with or without  $4 \mu\text{g ml}^{-1}$  hepsin for 24 h. Scale bar in a)–d) is  $5 \mu\text{m}$ . The concentration of all peptides is  $100 \mu\text{M}$ . Hepsin structure was obtained from RCSB protein data bank (PDB code 5ce1).<sup>[50]</sup>

**DMN-SGIPL** peptide was not recognized or cleaved by hepsin (Figure S21), emphasizing the essential role of the hepsin recognition site in the condensates formation process. CLSM results (Figure 4b–d) indicated that mutations in any component of the self-assembly motif, hepsin-binding motif, or hepsin recognition motif led to a complete absence of LLPS. The impaired condensates formation observed with **DMN-GIPL** highlighted the necessity of hydrophobic interactions during the initial condensation phase of LLPS. In contrast, the effects seen with **DMN-SGIPL** illustrated that enzymatic responsibility is critical for initiating condensates formation. The failure to construct in vitro condensates with **DMN-SGIPL** further demonstrated the importance of the hepsin recognition and binding motifs for effective peptide–protein interactions. These findings elucidate a clear structure–activity relationship

(SAR), indicating that the cooperative functionality of these peptide motifs is vital for the formation and stability of membraneless organelles in a cellular context. The interplay among self-assembly, enzymatic action, and multivalency reinforces the complexity of LLPS and highlights the necessity of each motif for achieving effective condensates dynamics. This SAR analysis provides insights into the molecular mechanisms underlying condensates formation and emphasizes the potential for designing peptides with tailored functionalities for specific applications in synthetic biology.

Hydrolysate **DMN-KQR-IPL** was also synthesized (Figure S22). In vitro condensates formation experiment (Figure S23) showed that hydrolysate could not form condensates with hepsin. Only aggregates were observed in CLSM images.

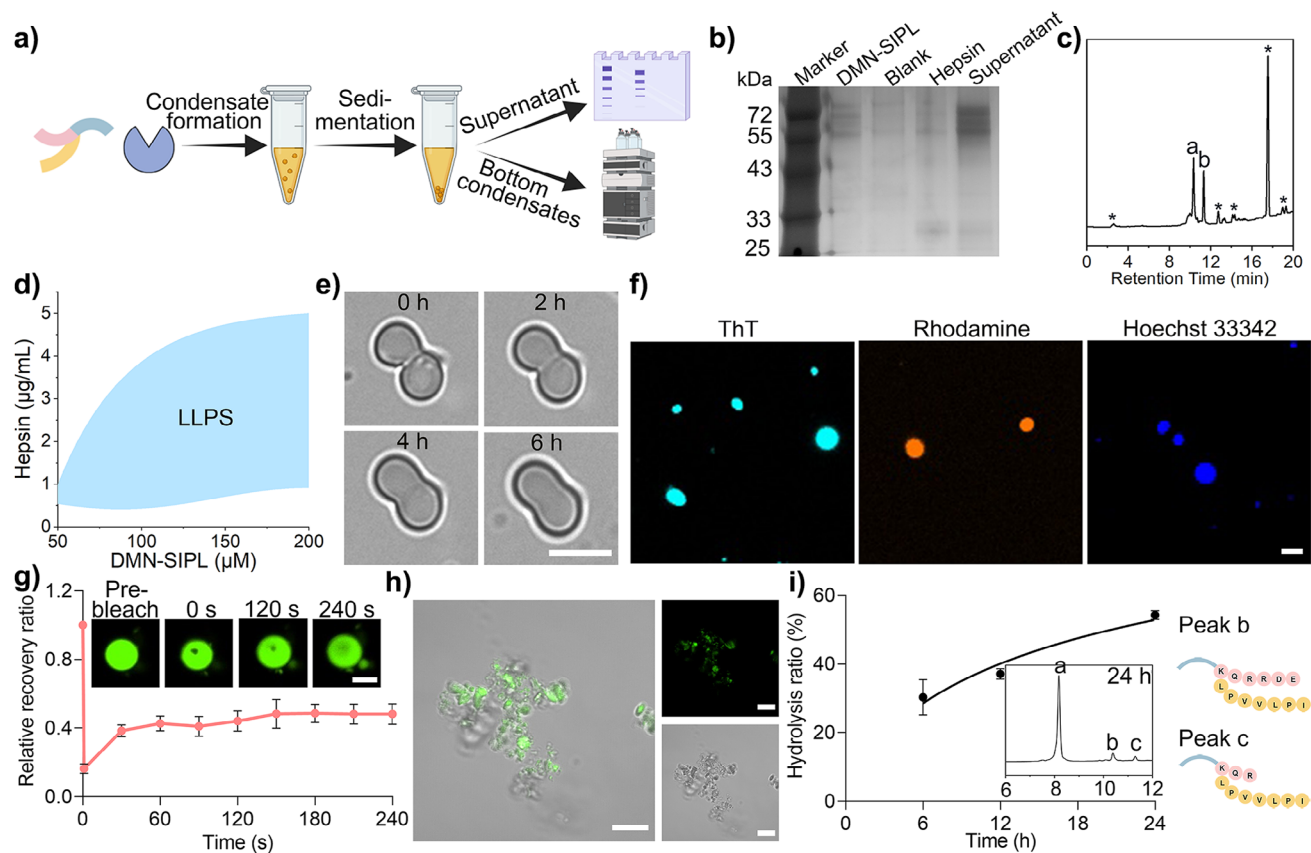


**Figure 5.** a) Schematic illustration of sedimentation assay to investigate the condensates composition in vitro. Condensates were formed using the described method, and sedimentation was employed to separate the condensates from the supernatant. The condensates were dissolved and analyzed by HPLC. The hepsin level in the supernatant was detected using silver staining SDS-PAGE. This figure was created with BioRender.com. b) Silver-stained SDS-PAGE of single **DMN-SIPL**, blank solution,  $4 \mu\text{g ml}^{-1}$  hepsin and the supernatant from the condensates formation solution. c) Analytic HPLC result of bottom condensates. Peaks a and b represent **DMN-SIPL** and **DMN-KQR-IPL**, respectively. Asterisks (\*) labels the analytic HPLC systematic peaks. d) Phase diagram of **DMN-SIPL** with different concentrations peptide and hepsin. The solution was incubated at  $37^\circ\text{C}$  for 24 h. e) Fusion process of condensates formed by **DMN-SIPL** ( $100 \mu\text{M}$ ) co-incubated with hepsin at  $37^\circ\text{C}$ . Scale bar is  $5 \mu\text{m}$ . f) CLSM images of condensates showing ThT, rhodamine, and Hoechst 33342 loading. Scale bar is  $5 \mu\text{m}$ . g) Fluorescence recovery after bleaching of condensates shown in f) ( $n = 7$ , error bar indicates SD). Scale bar is  $2 \mu\text{m}$ . h) CLSM images of  $100 \mu\text{M}$  **DMN-SIPL** co-incubated with hepsin and hepsin-inhibitor HepIn ( $10 \mu\text{M}$ ). Scale bar is  $5 \mu\text{m}$ . i) Quantification of **DMN-SIPL** hydrolysis and HPLC spectrum of **DMN-SIPL** ( $100 \mu\text{M}$ ) after treatment with  $4 \mu\text{g ml}^{-1}$  hepsin for different time points. Peak a represents internal control **DMN-GIPL**. Peak b represents **DMN-SIPL**. Peak c represents **DMN-KQR-IPL** ( $n = 3$ , error bar indicates SD).

The critical aggregation concentration (CAC) of **DMN-SIPL** and its hydrolysate were measured. The DLS results (Figure S24) indicated that the CAC value of hydrolysate **DMN-KQR-IPL** was lower than that of **DMN-SIPL**, suggesting that **DMN-KQR-IPL** has better self-assembly properties and increased hydrophobicity. Based on this, we hypothesized that hydrolysate may be too hydrophobic to interact with hepsin to form condensates. We synthesized peptides with different N-terminal capping groups (Figures S25 and S26) to assess their influence on condensate formation. Replacing DMN with acetic acid produced **Ac-SIPL**, which exhibited weaker self-assembly properties. In vitro results (Figure S27) showed that **Ac-SIPL** forms condensates in the presence of hepsin, indicating that tryptophan-tyrosine-phenylalanine sequence contributes to hydrophobicity for condensate formation. Analytic HPLC results indicated that the original **Ac-SIPL** peptide was hardly detectable after the addition of hepsin, indicating complete hydrolysis (Figure S28).

We also synthesized **ATH-SIPL** by replacing DMN with 9-anthracenecarboxylic acid (ATH), a more hydrophobic capping group (Figure S26). In vitro experiments showed that **ATH-SIPL** formed aggregates in the presence of hepsin (Figure S27), further suggesting that the N-terminal capping group significantly influences condensate formation. Overall, the hydrophobicity and steric hindrance of the N-terminal capping group are crucial for hydrolysis and condensate formation.

To investigate the composition of condensates in vitro, a sedimentation experiment was performed, followed by HPLC and SDS-PAGE analysis (Figure 5a). Silver-stained SDS-PAGE results (Figures 5b and S29) indicated a decrease in hepsin levels in the supernatant compared to the same concentration of hepsin alone, confirming that hepsin was a component of the condensates formed in vitro. Additionally, the analytical HPLC spectra of the bottom condensates (Figure 5c) revealed the presence of **DMN-SIPL** and its

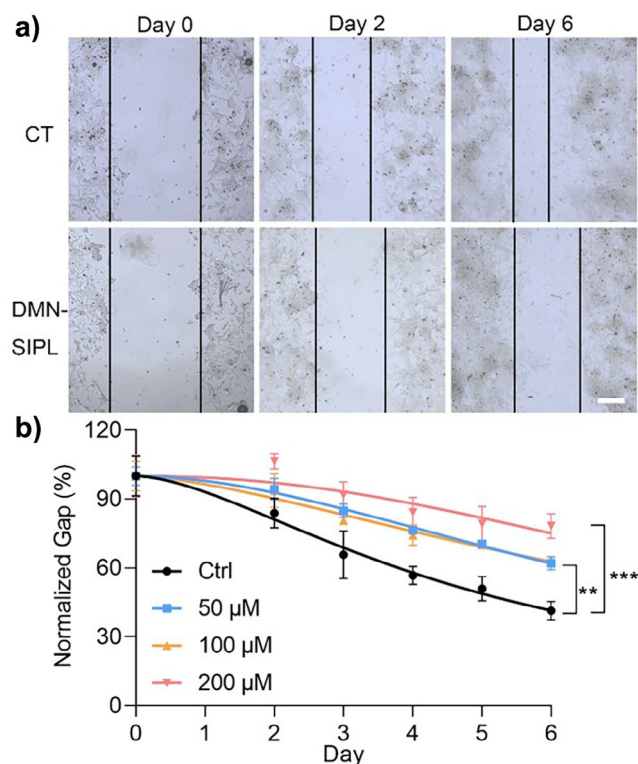


**Figure 6.** a) Wound-healing assay of LNCaP cells treated with culture medium and **DMN-SIPL** (100  $\mu\text{M}$ ) over 6 days. Scale bar is 100  $\mu\text{m}$ . b) Quantification of wound closure results ( $n = 3$ , error bar indicates SD).  $**P < 0.005$ ,  $***P < 0.0005$ .

hydrolysate, **DMN-KQR-IPL**. These findings suggested that the condensates consist of hepsin, **DMN-SIPL** and the hydrolysate **DMN-KQR-IPL**.

To further explore the phase behavior of **DMN-SIPL**, we conducted condensates formation experiments under various conditions. The phase diagram (Figure 5d) illustrated the phase behavior of the peptide system across different concentrations of **DMN-SIPL** and hepsin. LLPS was observed only within specific concentration ranges of both peptide and enzyme (Figure S30). At lower peptide concentrations, LLPS occurred with a low concentration of hepsin. As the peptide concentration increased, a wider range of hepsin concentration was effective in triggering LLPS. This positive correlation between peptide and hepsin concentrations likely resulted from the balance between peptide–peptide and peptide–enzyme interactions. Additionally, the size of condensates formed under varying conditions exhibited concentration-dependent increase (Figure S30). This phenomenon may be attributed to higher peptide concentrations, which promote the formation of more condensates and increase the likelihood of condensates fusion. For a fixed peptide concentration, the hydrolysis ratio of **DMN-SIPL** increased in an enzyme-dependent manner, enhancing its self-assembly properties. Concurrently, peptide–enzyme interactions were strengthened at higher hepsin concentrations. However, at elevated hepsin levels, the high hydrolysis ratio of **DMN-SIPL** (Figures S31 and S32) ultimately led to precipitation instead of condensates formation.

These results suggest that the balance between peptide–peptide interactions, peptide–enzyme interactions, and the hydrolysis ratio is critical for enzyme-induced LLPS. The phase diagram provides a comprehensive understanding of the enzyme-induced LLPS system, offering valuable insights into the underlying mechanisms governing condensates formation. Time-lapse bright-field microscopy was conducted to investigate condensates fusion in vitro (Figure 5e). The fusion process for this peptide–protein condensates system required approximately 6 h, indicating limited fluidity of the condensates. The uptake of guest molecules serves as strong evidence for characterizing liquid–liquid phase separation (LLPS). To assess this, we employed ThT, rhodamine, and Hoechst 33342 as fluorescent guest molecules. CLSM results (Figure 5f) demonstrated that these guest molecules were concentrated within the condensates, confirming the integrity of the LLPS. Fluorescence recovery after photobleaching (FRAP) was also performed to evaluate the properties of the condensates. The FRAP analysis (Figure 5g) revealed a slow and partial recovery ratio, suggesting that the fluidity of the condensates was poor. FRAP experiment was also conducted with condensates formed under various conditions. The FRAP result (Figure S33) showed negligible fluorescence recovery across all tested conditions, regardless of the concentration of peptide or hepsin. These results indicate that limited mobility may be attributed to the strong interactions between the peptide and hepsin, leading to notable stability and solid-like behavior of the condensates.<sup>[51–53]</sup> Another possible reason for the solid-like property might be that condensates gradually mature during the formation process. Understanding these interactions is crucial, as solid-like condensates may have a complementary role to liquid condensates in biological processes, potentially influencing their functionality and stability. To further investigate the role of hepsin in condensates formation, we co-incubated the hepsin inhibitor with **DMN-SIPL** and hepsin in vitro. CLSM results (Figure 5h) indicated that condensates formation was significantly suppressed in the presence of the inhibitor, with only peptide aggregates observed. This finding underscores the indispensable role of hepsin in facilitating condensates formation. Additionally, we assessed the enzymatic activity of the peptide using the internal standard method (Figures 5i, S31, and S34). **DMN-GIPL** was chosen as an internal control of **DMN-SIPL**. After 6 h of incubation with hepsin, hydrolysis product appeared, specifically at the cleavage site between two arginine residues (Figure S34). As the incubation time increased, the hydrolysis ratio of the peptide reached approximately 60% at 24 h, highlighting the significant enzymatic activity of hepsin in this system. Collectively, these results illustrate the critical role of hepsin in both the formation and stabilization of **DMN-SIPL** condensates, providing insights into the dynamics of LLPS in a cellular context.

#### Impact of Condensates to Cell Migration and Hepsin Signal Transduction

To investigate the impact of condensates formation on cancer cell migration, we conducted a wound-healing assay

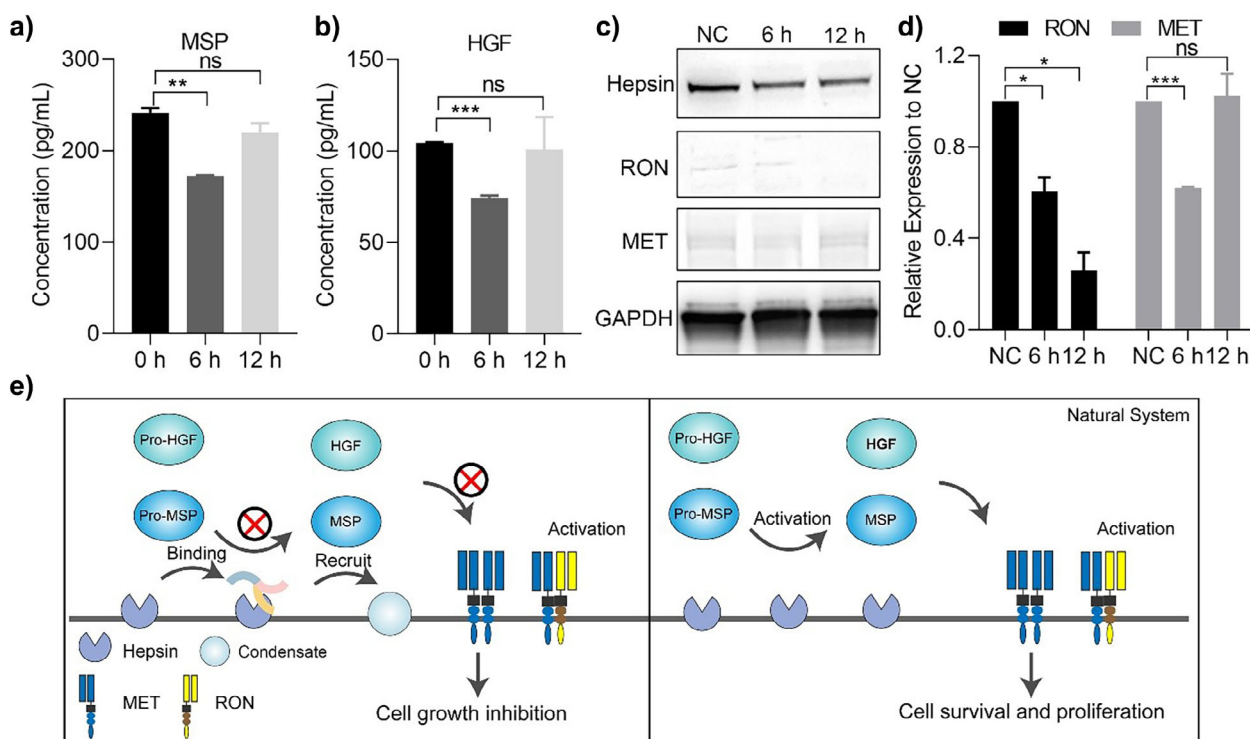


**Figure 7.** Concentrations of secreted a) MSP, and b) HGF in the culture medium of LNCaP cells treated with **DMN-SIPL** (100  $\mu$ M) for 6 and 12 h ( $n = 3$ , error bar indicates SD). c) Western blot result of hepsin downstream proteins after 6 and 12 h **DMN-SIPL** (100  $\mu$ M) treatment. d) Quantification of relative protein expression in western blot ( $n = 2$ , error bar indicates SD). e) Mechanism of **DMN-SIPL** influences hepsin signaling pathways. Condensates formation inhibited the upstream proteins activation and downstream signal transduction. ns,  $P > 0.05$ ; \* $P < 0.05$ ; \*\* $P < 0.005$ ; \*\*\* $P < 0.0005$ .

(Figure 6). This assay allows for the assessment of cell motility and the potential inhibitory effects of **DMN-SIPL** on cell migration. After 48 h, significant differences in wound closure were observed between cells treated high concentration of **DMN-SIPL** and untreated cells. Specifically, by day 6, the wound area in the control group, which received no treatment, had reduced to approximately 40% of its original size (day 0, Figure 6b). In contrast, the group treated with different concentrations **DMN-SIPL** (Figure S35) showed a marked suppression of cell migration, indicating that the addition of **DMN-SIPL** significantly impeded the healing process. These results suggested that **DMN-SIPL** not only alters the physical properties of the cells but also played a crucial role in modulating cellular behaviors associated with migration. This inhibition of migration could be particularly relevant in the context of cancer metastasis, where the ability of tumor cells to migrate and invade surrounding tissues is a key factor in disease progression.

In a natural system, hepsin plays a crucial role in cleaving inactive pro-hepatocyte growth factor (pro-HGF) and pro-mesenchymal stem cell protein (pro-MSP) to their active forms, HGF and MSP, respectively.<sup>[37]</sup> These ligands subsequently induce dimerization of the MET and RON receptors, activating downstream signaling pathways that promote cell proliferation. Therefore, the concentrations of MSP and HGF can serve as indicators of active hepsin levels on the cell membrane.<sup>[54]</sup> Activation of MSP-RON signaling promotes wound healing and invasive tumor growth.<sup>[55,56]</sup>

The ELISA results (Figure 7a,b) showed a significant decrease in MSP and HGF concentrations following co-cubation with **DMN-SIPL**, particularly noticeable at the 6 h mark. At this time point, the formation of condensates was already observed, which may correlate with the sharp decline in MSP and HGF levels. This reduction suggested that **DMN-SIPL** effectively inhibits the activation of pro-MSP and pro-HGF, thereby limiting the production of its downstream ligands. Complementary Western blot analysis (Figure 7c) further indicated a notable decrease in hepsin levels after **DMN-SIPL** treatment. This decrease could be attributed to two potential mechanisms: first, **DMN-SIPL** may hinder the activation of pro-MSP and pro-HGF by reducing the availability of active hepsin; second, hepsin may become sequestered within the condensates formed by **DMN-SIPL**, preventing it from cleaving extracellular substrates. The Western blot results (Figures 7c,d and S36) also revealed a clear reduction in hepsin expression, suggesting a consequential inhibition of hepsin-dependent signaling pathways. Notably, the levels of RON and MET proteins exhibited similar decreasing trends, reinforcing the notion that the inhibition of hepsin leads to downstream signaling disruption.

Collectively, these findings indicate that the condensates formation involving **DMN-SIPL** and hepsin effectively inhibits the activation of upstream proteins, thereby blocking the transduction of hepsin-associated signaling pathways. This disruption could have significant implications for cellular behaviors linked to proliferation and migration, suggesting

that targeting condensates dynamics may offer a novel therapeutic strategy in managing conditions where hepsin is implicated.

## Conclusion

In summary, this work describes a significant advance in the engineering of the amphiphilic branched peptide, demonstrating the ability to construct peptide condensates in living cells through enzymatic interactions with hepsin. Our findings reveal that the formation of these condensates not only sequesters hepsin but also significantly reduces the activation of upstream signaling proteins, including pro-hepatocyte growth factor (pro-HGF) and pro-mesenchymal stem cell protein (pro-MSP). This reduction in active HGF and MSP disrupts critical signaling pathways that drive cancer cell migration. The ability to design peptides that induce condensates formation in response to enzymatic activity is crucial for advancing therapeutic strategies. Through in vitro condensates formation experiment, we conclude that the balance of peptide–peptide interactions, peptide–protein interaction, and hydrolysis ratio in the system is essential for achieving enzyme-induced LLPS process.

This study underscores the importance of engineering peptide-based systems to modulate condensates formation within living cells. By targeting hepsin activity and the resulting condensates dynamics, this work provides an efficient approach for inhibiting tumor metastasis and enhancing our understanding of cellular biochemical processes. These findings highlight the transformative potential of peptide-based interventions in manipulating biological systems for therapeutic applications.

## Supporting Information

General materials, peptide synthesis, cell culture, immunofluorescence, hydrolysis in cells and in vitro, subcellular distribution and cellular uptake of peptide, endocytosis determination, preparation of condensates in vitro, critical aggregation concentration measurement, guest molecule partitioning, fluorescence recovery after photobleaching, silver-stained SDS-PAGE, wound healing experiment, MSP and HGF level in culture medium, and Western blotting.

## Acknowledgements

This project was supported by the National Natural Science Foundation of China (82272145). This research was supported by the Instrumentation and Service Centers for Molecular Science and for Physical Science, respectively, as well as by the Biomedical Research Core Facilities at Westlake University. The authors also thank Laicheng Zhou for the assistance with the synthesis of DMN.

## Conflict of Interests

The authors has applied a patent based on this work.

## Data Availability Statement

The data that support the findings of this study are available from the corresponding author upon reasonable request.

**Keywords:** Condensates • Droplet • Liquid–liquid phase separation • Peptide • Self-assembly

- [1] L. Tang, *Nat. Methods* **2019**, *16*, 18–18.
- [2] Z. Xu, W. Wang, Y. Cao, B. Xue, *Supramol. Mater.* **2023**, *2*, 100049.
- [3] S. Alberti, A. A. Hyman, *Nat. Rev. Mol. Cell Biol.* **2021**, *22*, 196–213.
- [4] Y. Dai, L. You, A. Chilkoti, *Nat. Rev. Bioeng.* **2023**, *1*, 466–480.
- [5] J. L. Silva, D. Foguel, V. F. Ferreira, T. C. R. G. Vieira, M. A. Marques, G. D. S. Ferretti, T. F. Outeiro, Y. Cordeiro, G. A. P. de Oliveira, *Chem. Rev.* **2023**, *123*, 9094–9138.
- [6] S. Alberti, A. Gladfelter, T. Mittag, *Cell* **2019**, *176*, 419–434.
- [7] J. B. Woodruff, A. A. Hyman, E. Boke, *Trends Biochem. Sci.* **2018**, *43*, 81–94.
- [8] Z. Wang, J. Lou, H. Zhang, *J. Biol. Chem.* **2022**, *298*, 101782.
- [9] S. Yu, W. Chen, G. Liu, B. Flores, E. L. DeWolf, B. Fan, Y. Xiang, M. J. Webber, *J. Am. Chem. Soc.* **2024**, *146*, 7498–7505.
- [10] J. Wang, L. Hu, H. Zhang, Y. Fang, T. Wang, H. Wang, *Adv. Mater.* **2022**, *34*, 2104704.
- [11] C. P. Brangwynne, C. R. Eckmann, D. S. Courson, A. Rybarska, C. Hoege, J. Gharakhani, F. Jülicher, A. A. Hyman, *Science* **2009**, *324*, 1729–1732.
- [12] S. F. Banani, H. O. Lee, A. A. Hyman, M. K. Rosen, *Nat. Rev. Mol. Cell Biol.* **2017**, *18*, 285–298.
- [13] A. A. Hyman, K. Simons, *Science* **2012**, *337*, 1047–1049.
- [14] E. B. Wilson, *Science* **1899**, *10*, 33–45.
- [15] S. Mehta, J. Zhang, *Nat. Rev. Cancer* **2022**, *22*, 239–252.
- [16] B. Van Treeck, R. Parker, *Cell* **2018**, *174*, 791–802.
- [17] A. G. Larson, D. Elnatan, M. M. Keenen, M. J. Trnka, J. B. Johnston, A. L. Burlingame, D. A. Agard, S. Redding, G. J. Narlikar, *Nature* **2017**, *547*, 236–240.
- [18] P. Li, S. Banjade, H.-C. Cheng, S. Kim, B. Chen, L. Guo, M. Llaguno, J. V. Hollingsworth, D. S. King, S. F. Banani, P. S. Russo, Q.-X. Jiang, B. T. Nixon, M. K. Rosen, *Nature* **2012**, *483*, 336–340.
- [19] M. Du, Z. J. Chen, *Science* **2018**, *361*, 704–709.
- [20] M. Abbas, W. P. Lipiński, J. Wang, E. Spruijt, *Chem. Soc. Rev.* **2021**, *50*, 3690–3705.
- [21] A. Jain, S. Kassem, R. S. Fisher, B. Wang, T.-D. Li, T. Wang, Y. He, S. Elbaum-Garfinkle, R. V. Uljin, *J. Am. Chem. Soc.* **2022**, *144*, 15002–15007.
- [22] Q. Guo, G. Zou, X. Qian, S. Chen, H. Gao, J. Yu, *Nat. Commun.* **2022**, *13*, 5771.
- [23] M. Abbas, W. P. Lipiński, K. K. Nakashima, W. T. Huck, E. Spruijt, *Nat. Chem.* **2021**, *13*, 1046–1054.
- [24] A. Baruch Leshem, S. Sloan-Dennison, T. Massarano, S. Ben-David, D. Graham, K. Faulds, H. E. Gottlieb, J. H. Chill, A. Lampel, *Nat. Commun.* **2023**, *14*, 421.
- [25] J. Liu, F. Zhorabek, X. Dai, J. Huang, Y. Chau, *ACS Cent. Sci.* **2022**, *8*, 493–500.
- [26] S. Cao, T. Ivanov, J. Heuer, C. T. J. Ferguson, K. Landfester, L. Caire da Silva, *Nat. Commun.* **2024**, *15*, 39.
- [27] Y. Sun, S. Y. Lau, Z. W. Lim, S. C. Chang, F. Ghadessy, A. Partridge, A. Miserez, *Nat. Chem.* **2022**, *14*, 274–283.
- [28] R. Kubota, S. Torigoe, I. Hamachi, *J. Am. Chem. Soc.* **2022**, *144*, 15155–15164.

- [29] J. Liu, E. Spruijt, A. Miserez, R. Langer, *Nat. Rev. Mater.* **2023**, *8*, 139–141.
- [30] H. Chen, Y. Bao, X. Li, F. Chen, R. Sugimura, X. Zeng, J. Xia, *Angew. Chem. Int. Ed.* **2024**, *63*, e202410566.
- [31] Y. Shin, J. Berry, N. Pannucci, M. P. Haataja, J. E. Toettcher, C. P. Brangwynne, *Cell* **2017**, *168*, 159–171.e14.
- [32] H. Nakamura, A. A. Lee, A. S. Afshar, S. Watanabe, E. Rho, S. Razavi, A. Suarez, Y.-C. Lin, M. Tanigawa, B. Huang, R. Derose, D. Bobb, W. Hong, S. B. Gabelli, J. Goutsias, T. Inoue, *Nat. Mater.* **2018**, *17*, 79–89.
- [33] Z. Feng, H. Wang, B. Xu, *J. Am. Chem. Soc.* **2018**, *140*, 16433–16437.
- [34] Y. Ding, D. Zheng, L. Xie, X. Zhang, Z. Zhang, L. Wang, Z.-W. Hu, Z. Yang, *J. Am. Chem. Soc.* **2023**, *145*, 4366–4371.
- [35] J. Kim, S. Lee, Y. Kim, M. Choi, I. Lee, E. Kim, C. G. Yoon, K. Pu, H. Kang, J. S. Kim, *Nat. Rev. Mater.* **2023**, *8*, 710–725.
- [36] S. Kim, J.-B. Chae, D. Kim, C.-W. Park, Y. Sim, H. Lee, G. Park, J. Lee, S. Hong, B. Jana, C. Kim, H. Chung, J.-H. Ryu, *J. Am. Chem. Soc.* **2023**, *145*, 21991–22008.
- [37] S. Li, L. Wang, S. Sun, Q. Wu, *The FEBS J.* **2021**, *288*, 5252–5264.
- [38] L. Lu, A. Cole, D. Huang, Q. Wang, Z. Guo, W. Yang, J. Lu, *Biomolecules* **2022**, *12*, 203.
- [39] T. A. Tervonen, S. M. Pant, D. Belitškin, J. I. Englund, K. Närhi, C. Haglund, P. E. Kovanen, E. W. Verschuren, J. Klefström, *Cancer Res.* **2021**, *81*, 1513–1527.
- [40] M. H. Kang, M. J. Park, H. J. Yoo, K. Y. hyuk, S. G. Lee, S. R. Kim, D. W. Yeom, M. J. Kang, Y. W. Choi, *Eur. J. Pharm. Biopharm.* **2014**, *87*, 489–499.
- [41] A. S. Murray, F. A. Varela, K. List, *Biol. Chem.* **2016**, *397*, 815–826.
- [42] O. Klezovitch, J. Chevillet, J. Mirosevich, R. L. Roberts, R. J. Matusik, V. Vasioukhin, *Cancer Cell* **2004**, *6*, 185–195.
- [43] L. Hu, Y. Li, X. Lin, Y. Huo, H. Zhang, H. Wang, *Angew. Chem. Int. Ed.* **2021**, *60*, 21807–21816.
- [44] H. Liu, Z. Song, Y. Zhang, B. Wu, D. Chen, Z. Zhou, H. Zhang, S. Li, X. Feng, J. Huang, H. Wang, *Nat. Mater.* **2025**, 1–12, <https://doi.org/10.1038/s41563-025-02164-3>.
- [45] L. C. Nelemans, L. Gurevich, *Materials* **2020**, *13*, 366.
- [46] R. Mout, M. Ray, G. Yesilbag Tonga, Y.-W. Lee, T. Tay, K. Sasaki, V. M. Rotello, *ACS Nano* **2017**, *11*, 2452–2458.
- [47] V. Bandmann, A. S. Mirsanaye, J. Schäfer, G. Thiel, T. Holstein, M. Mikosch-Wersching, *Sci. Rep.* **2019**, *9*, 12999.
- [48] M. Koivusalo, C. Welch, H. Hayashi, C. C. Scott, M. Kim, T. Alexander, N. Touret, K. M. Hahn, S. Grinstein, *J. Cell Biol.* **2010**, *188*, 547–563.
- [49] P. Panja, N. R. Jana, *J. Phys. Chem. B* **2020**, *124*, 5323–5333.
- [50] K. N. Rao, R. C. Anita, R. Sangeetha, L. Anirudha, H. Subramnay, Worldwide Protein Data Bank, **2016**.
- [51] A. Molliex, J. Temirov, J. Lee, M. Coughlin, A. P. Kanagaraj, H. J. Kim, T. Mittag, J. P. Taylor, *Cell* **2015**, *163*, 123–133.
- [52] A. Patel, H. O. Lee, L. Jawerth, S. Maharana, M. Jahnel, M. Y. Hein, S. Stoynev, J. Mahamid, S. Saha, T. M. Franzmann, A. Pozniakovski, I. Poser, N. Maghelli, L. A. Royer, M. Weigert, E. W. Myers, S. Grill, D. Drechsel, A. A. Hyman, S. Alberti, *Cell* **2015**, *162*, 1066–1077.
- [53] C. N. Hernandez-Candia, B. R. Brady, E. Harrison, C. L. Tucker, *Nat. Chem. Biol.* **2024**, *20*, 452–462.
- [54] W. Ming-Hai, Z. Ruiwen, Z. Yong-Qing, Y. Hang-Ping, *J. Biomed. Res.* **2013**, *27*, 345–356.
- [55] R. Ganesan, G. A. Kolumam, S. J. Lin, M.-H. Xie, L. Santell, T. D. Wu, R. A. Lazarus, A. Chaudhuri, D. Kirchhofer, *Mol. Cancer Res.* **2011**, *9*, 1175–1186.
- [56] H.-P. Yao, Y.-Q. Zhou, R. Zhang, M.-H. Wang, *Nat. Rev. Cancer* **2013**, *13*, 466–481.

Manuscript received: March 02, 2025

Revised manuscript received: April 30, 2025

Accepted manuscript online: May 18, 2025

Version of record online: ■■■■■

## Research Article

## Peptides

Y. Li, T. Xu, Y. Li, H. Wang\* — e202504958

Enzyme Induced Solid-Like Condensates  
Formation of Engineered Peptide in Living  
Cells for Prostate Cancer Inhibition

This study presents the condensate formation from engineered amphiphilic-branched peptides in living cells through enzymatic reactions. We describe the rational design and synthesis of DMN-SIPL, a peptide that forms solid-like condensates via liquid–liquid phase separation (LLPS) when triggered by the type-II membrane-associated serine peptidase hepsin.

